DOT/FAA/TC-22/4

Federal Aviation Administration
William J. Hughes Technical Center
Aviation Research Division
Atlantic City International Airport
New Jersey 08405

Reflective Crack Propagation Model—Part 2: Mode II

March 2022

Final Report

This document is available to the U.S. public through the National Technical Information Services (NTIS), Springfield, Virginia 22161.

This document is also available from the Federal Aviation Administration William J. Hughes Technical Center at actlibrary.tc.faa.gov.

U.S. Department of Transportation
Federal Aviation Administration

NOTICE

This document is disseminated under the sponsorship of the U.S. Department of Transportation in the interest of information exchange. The United States Government assumes no liability for the contents or use thereof. The United States Government does not endorse products or manufacturers. Trade or manufacturer's names appear herein solely because they are considered essential to the objective of this report. The findings and conclusions in this report are those of the author(s) and do not necessarily represent the views of the funding agency. This document does not constitute FAA policy. Consult the FAA sponsoring organization listed on the Technical Documentation page as to its use.

This report is available at the Federal Aviation Administration William J. Hughes Technical Center’s Full-Text Technical Reports page: actlibrary.tc.faa.gov in Adobe Acrobat portable document format (PDF).

Technical Report Documentation Page

1. Report No.	2. Government Accession No.	3. Recipient's Catalog No.
DOT/FAA/TC-22/4		

4. Title and Subtitle	5. Report Date
REFLECTIVE CRACK PROPAGATION MODEL—PART 2: MODE II	March 2022
	6. Performing Organization Code ANG-E262
7. Author(s) Kairat Tuleubekov	8. Performing Organization Report No.
9. Performing Organization Name and Address General Dynamics Information Technology 600 Aviation Research Blvd. Egg Harbor Township, NJ 08234	10. Work Unit No. (TRAIS)
	11. Contract or Grant No.
12. Sponsoring Agency Name and Address U.S. Department of Transportation Federal Aviation Administration Airport Engineering Division 800 Independence Ave., SW Washington, DC 20591	13. Type of Report and Period Covered Final Report
	14. Sponsoring Agency Code AAS-100

15. Supplementary Notes

The Federal Aviation Administration Aviation Research Division COR was Jeffrey Gagnon.

16. Abstract

The Federal Aviation Administration (FAA) developed a two-dimensional model of its full-scale, indoor, reflection cracking test equipment at the National Airport Pavement Test Facility (NAPTF), William J. Hughes Technical Center, Atlantic City International Airport, NJ. The analytical model represents two jointed concrete slabs and a continuous hot mix asphalt overlay with a single, preexisting vertical crack centered on the joint. Mode II stress intensity factors (SIF) were derived from superposition of the linear elastic solutions of two separate problems having different domains. The first problem considers the uncracked domain with the same prescribed vertical displacements at the bottom as the original problem. The second problem considers the cracked domain, where vertical displacements at the bottom boundary are prescribed to be zero. The sum of the solutions of these two problems in the linear elastic domain gives the desired Mode II solution at the vicinity of the crack tip. By applying Schapery's theory of crack propagation in viscoelastic materials, this model can be used to determine the energy release rate (ERR) in and asphalt overlay subject to Mode II cracking caused by repeated aircraft traffic loads. The model was used to compute Mode II SIFs at the crack tip for a series of incremental crack lengths, using assumed properties. Computed SIF values showed good agreement with SIF values computed by a finite element model (ABAQUS).

17. Key Words	18. Distribution Statement
Reflection cracking, Asphalt overlay, Airport pavement, Viscoelasticity, Fracture mechanics	This document is available to the U.S. public through the National Technical Information Service (NTIS), Springfield, Virginia 22161. This document is also available from the Federal Aviation Administration William J. Hughes Technical Center at actlibrary.tc.faa.gov.

19. Security Classif. (of this report)	20. Security Classif. (of this page)	21. No. of Pages	22. Price
Unclassified	Unclassified	30	

TABLE OF CONTENTS

LIST OF FIGURES

LIST OF ACRONYMS

2D	Two dimensional
AC	Asphalt concrete
ERR	Energy release rate
FAA	Federal Aviation Administration
FEM	Finite element method
NAPTF	National Airport Pavement Test Facility
NTIS	National Technical Information Services
PDF	Portable document format
SIF	Stress intensity factor

EXECUTIVE SUMMARY

The Federal Aviation Administration (FAA) provides standards for the thickness design of hot mix asphalt (HMA) overlays on rigid airport pavements. The current FAA design procedure does not explicitly consider the important reflection cracking distress mode. Reflection cracks commonly result from temperature-induced cyclic contraction (opening) and expansion (closing) in the concrete slab but may also have a traffic-induced component. This report describes an FAA study that models crack propagation for the case of traffic-induced cyclic joint opening (Mode II fracture), whereas temperature-induced joint opening was studied earlier in its companion report, DOT/FAA/TC-20/17.

The companion report used the developed model to determine Mode I Paris Law parameters using experimental data from the National Airport Pavement Test Facility (NAPTF). A similar exercise was not possible for the Mode II formulation, because (1) the rig does not accept wheeled traffic, and (2) in any case, traffic loads do not produce pure Mode II loading (it is combined Mode I/Mode II). However, it is expected that the analysis presented here will be applied to mixed-mode reflection crack prediction.

The elements of this study are mechanical formulation of the problem, definition of the material parameters for model implementation, modification of the crack propagation law (Paris' Law) for viscoelastic materials, the representation of the asphalt viscoelastic response by Prony series, and the assumption of displacement controlled cyclic loading. The assumption of displacement control makes the problem separable into an elastic part and a time-dependent part.

The viscoelastic asphalt material was represented in the model by its Prony series. The method to compute Prony terms is described in earlier report DOT/FAA/TC-20/17 for Mode I crack propagation case and is common for Mode II, too.

Computing the energy release rate (ERR) in the modified crack propagation law requires information about viscoelastic tensile strains and forces. Because the tests are displacement-controlled, it was possible to separate time variables (e.g., normalized load history) from spatial variables (e.g., elastic strains). This immediately allows the original ERR to be decoupled into an elastic part and a time-domain part. The elastic solution proceeds by superposing of the linear elastic solutions of two separate problems with prescribed boundary displacements—one based on the intact overlay and the other on the cracked domain. The analytical solution presented gives values of Mode II stress intensity factors that are in agreement with those from a well-accepted Finite Element Methods program.

1. INTRODUCTION

This report describes the two-dimensional (2D) analytical modeling of a structure consisting of two jointed concrete slabs and an asphalt concrete (AC) overlay, which is subjected to traffic-induced mechanical loading. This type of load typically causes in-plane shear cracking (Mode II) within the overlay material.

An analytical model has advantages over an equivalent numerical model for both qualitative and quantitative analyses. Using the finite element method (FEM), a simple parametric sensitivity analysis involving three input parameters, and taking just 10 input values for each parameter, requires running $10^3 = 1000$ cases, each of which is time-consuming. To accelerate computation (at the expense of numerical accuracy), many authors have adopted a very coarse finite element mesh. For example, the finite element analysis package, CrackPro, uses only five points around the crack tip (Hu et al., 2008). By contrast, the analytical model discussed in this report achieves both computational efficiency and accuracy. The model can be used to compute the stress intensity factor (SIF) or energy release rate (ERR) in an asphalt overlay subject to Mode II cracking caused by aircraft traffic loads.

Consider the overlay of dimensionless length *2L* and thickness *h* with a preexisting vertical crack of length $a < h$ and constant Poisson's ratio $\nu = 0.35$, under assumptions of plane strain in two dimensions (length and thickness), and uniform crack propagation across the third dimension (width) of the overlay. The coordinate system has its origin *O* located just above the joint at the bottom surface of the overlay (Figure 1). The vertical axis (*x* axis) aligns with the crack, and the horizontal axis (*y* axis) coincides with the bottom surface of the overlay.

As discussed in a companion report about Mode I cracking (Tuleubekov, 2020), displacement-controlled boundary conditions dictate that when there is separation of time and spatial variables in displacement fields u_i:

$$u_i(t;\ x, y) = \ u_i^e(x, y)\Lambda(t) \tag{1}$$

where $i = 1,2;$ and $0 \leq \Lambda(t) \leq 1$ is the normalized amplitude of applied boundary displacement, and the superscript *e* refers to "elastic." Going forward, $u_i^e(x, y)$ is the displacement at location (x, y) when the maximum displacement u_0 is applied to the bottom of the overlay. Strains ε_{ij} are similarly separable:

$$\varepsilon_{ij}(t;\ x, y) = \ \varepsilon_{ij}^e(x, y)\Lambda(t) \tag{2}$$

Computationally, the most challenging part of this work is solving the elastic static problem formulated for the elastic (time-independent) variables $u_i^e,\ \varepsilon_{ij}^e$ in equations (1) and (2). A solution to this problem that makes use of complex analysis is presented in appendix B of this report. To reduce the number of independent variables under consideration, the original physical problem is reformulated into a dimensionless form (Figure 1), normalizing length quantities by the overlay thickness *h* and stress quantities by the instantaneous Young's modulus E_0 of asphalt material. Henceforth, all variables are given in dimensionless terms.

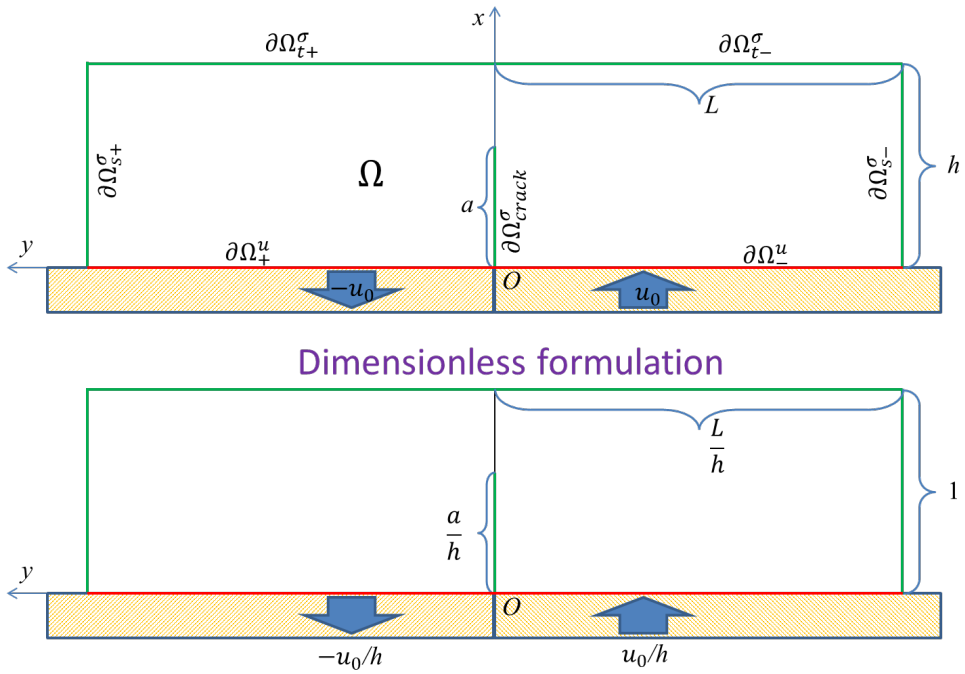

Figure 1. Original (top) and Dimensionless (bottom) Formulation of the Problem

2. DECOMPOSITION OF ELASTIC PROBLEM

The elastic problem is approached by superposition of solutions of the two problems illustrated in Figure 2. The first problem considers the uncracked domain with the same prescribed vertical displacements at the bottom as the original problem. The second problem considers the cracked domain; however, vertical displacements at the bottom boundary are zero. The sum of the solutions of these two problems (Figure 2) in the linear elastic domain will give the desired Mode II solution.

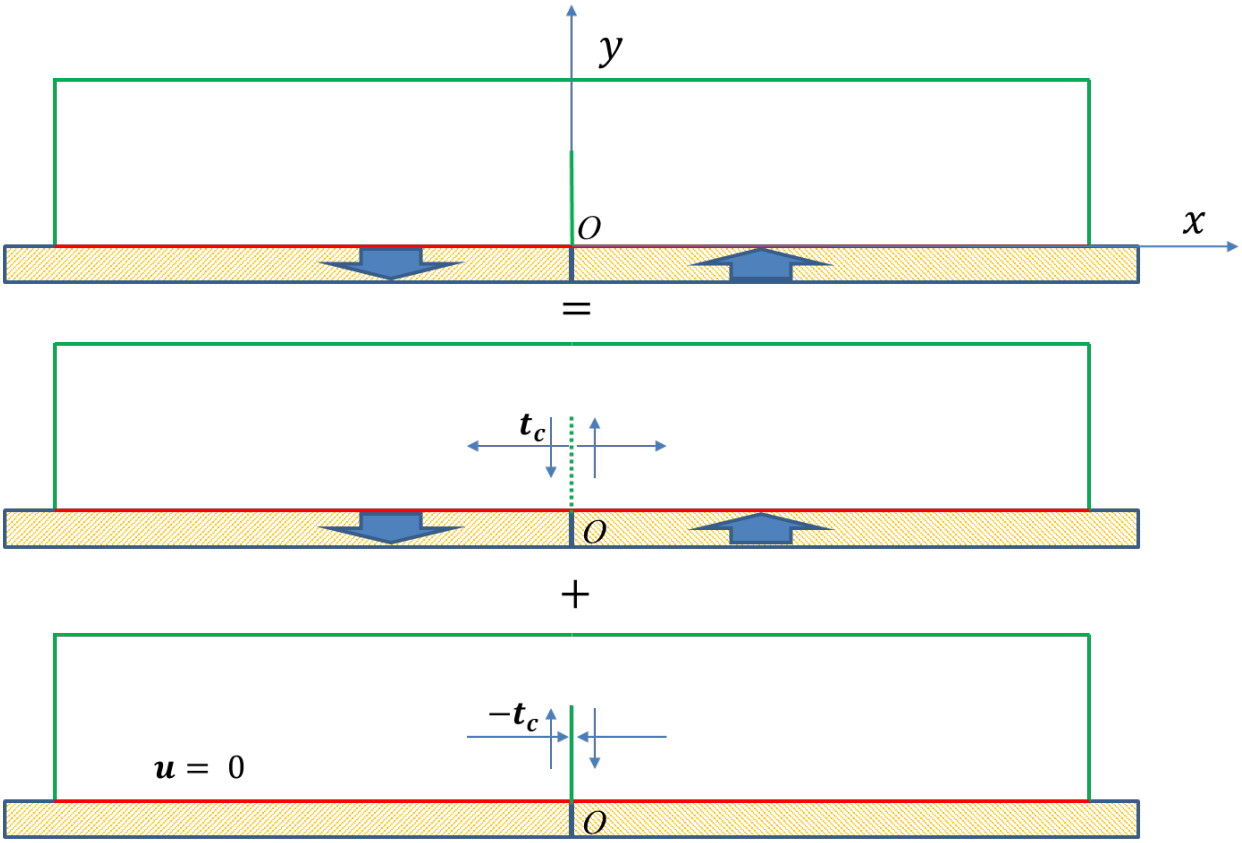

Figure 2. Decomposition of the Original Problem (top) into Subproblems Defined on Intact (middle) and Cracked (bottom) Domains

3. ASPHALT MATERIAL

The viscoelastic material is defined by a Prony series expansion of the relaxation modulus:

$$\frac{E(t)}{E_0} = 1 - \sum_{i=1}^{\infty} \frac{E_i}{E_0}\left(1 - e^{\frac{-t}{\tau_i}}\right) \tag{3}$$

where $E_0 = E(0)$ is the instantaneous modulus. With long-term modulus $E_\infty = E(\infty)$, it is useful to note that:

$$\sum_{i=1}^{\infty} E_i = E_0 - E_\infty$$

Equation (3) can be rewritten:

$$E(t) = E_\infty + \sum_{i=1}^{\infty} E_i e^{\frac{-t}{\tau_i}} \tag{4}$$

4. FAILURE LAW

In this section, Schapery's theory of crack damage in viscoelastic material is discussed. As described in Gu et al. (2015), within that theory's framework, Paris' law has a modified form:

$$\frac{da}{dn} = K\left(\frac{\partial W_R^c}{\partial A}\right)^{\mu} \tag{5}$$

where a is the current crack length, n is the current number of fatigue life cycles, ∂A is the area element of a newly created crack surface, and $\frac{\partial W_R^c}{\partial A}$ is the ERR per loading cycle of cumulative pseudo work W_R. That is, the cumulative sum of pseudo-work is:

$$W_R^c(n) = \sum_{k=1}^{n} W_R(k) \tag{6}$$

where $W_R(k)$ is the pseudo-work spent in the k-th load cycle $[t_{begin}, t_{end}]$ to further increment the crack. Fracture parameters K and μ are material parameters. The determination of K and μ from full-scale test data is the goal of the current research.

To operate with equation (5) freely, a good approximation $a(n)$ of measured crack length is needed at each point. In describing Mode I cracking, Tuleubekov (2020) used data from a full-scale testing rig at the Federal Aviation Administration (FAA) National Airport Pavement Test Facility (FAA, n.d.) that simulated reflective cracks due to temperature cycling only (pure Mode I). In the present case (Mode II), similar test measurements of crack length (and therefore crack propagation rate) caused purely by shear loading are lacking. Indeed, under traffic loading conditions, each wheel passage results in not just Mode II loading, but a mixture of Mode II with both Mode I and Mode III, and which mode is dominant depends on the wheel position with respect to the joint. For now, we will derive a general solution applicable to any particular set of crack propagation $a(n)$ data.

Let N denote the total number of cycles to fully separate the overlay (complete the crack). To fit the number of cumulative cycles n from the test data to corresponding crack lengths a, one may use a fifth-degree polynomial and its derivative:

$$a(n) = \sum_{k=1}^{5} a_k \left(\frac{n}{N} - 1\right)^k \tag{7}$$

$$\frac{da}{dn} = \frac{1}{N}\sum_{k=1}^{5} k a_k \left(\frac{n}{N} - 1\right)^{k-1} \tag{8}$$

where a_k are fitting coefficients.

As stated in the introduction, assume that the crack grows uniformly along the whole width b of the overlay. Under this assumption, the differential increment ∂A of the crack surface area is:

$$\partial A = 2b\ \partial a \tag{9}$$

where $\partial a = da$ is the differential increment of crack length. Having equations (8) and (9), and using the differentiation rule:

$$\frac{\partial W_R^c}{\partial A} = \frac{1}{2b}\frac{\partial W_R^c}{\partial a} = \frac{1}{2b}\frac{\partial W_R^c}{\partial n}\Big/\frac{\partial a}{\partial n} \tag{10}$$

we need only to find pseudo work W_R^c at each cycle n to insert it into equation (10) and then to the failure law, equation (5). The next section examines the derivation of cumulative pseudo work.

5. PSEUDO WORK

For the shear loading problem, the load $P_{VE}(t)$ described in Walubita et al. (2013) is adapted as follows. Introduce the load $P_{VE}(t)$ on load-displacement curves as the measured (viscoelastic) force for a specimen with thickness h and width b:

$$P_{VE}(t) = \iint_A \sigma_{xy}(t;\ x, 0, z)\ dx\ dz \tag{11}$$

where A is the intact area (cross-section $x > a, y = 0$ above the crack tip, Figure 1), and $\sigma_{xy}(t;\ x, 0, z)$ is the shear stress acting on the cross-sectional plane $y = 0$. For a crack of length a, we find that the intact area $= \{(x, z): a < x < h,\ 0 < z < b\}$, so:

$$P_{VE}(t) = \int_0^b \int_{a(n(t))}^h \sigma_{xy}(t;\ x, 0, z)\ dx\ dz \tag{12}$$

Recall that crack length indirectly depends on time. That dependence is implicit and is expressed via the number of cycles completed before the moment t. In the plane strain problem, the tensile stress $\sigma_{xy}(t;\ x, y, z)$ does not vary along width z, i.e.:

$$\frac{d}{dz}\ \sigma_{xy}(t;\ x, y, z) = 0$$

Then the external integral in equation (12) reduces to simple multiplication by width b:

$$P_{VE}(t) = b \int_{a(n(t))}^h \sigma_{xy}(t;\ x, 0)\ dx \tag{13}$$

where z is omitted henceforth. The viscoelastic stress is further calculated using the constitutive model for the uniaxial viscoelastic response, which is expressed as

$$\sigma_{xy}(t;\ x,0) = \frac{1}{1+\nu}\int_0^t E(t-\tau)\frac{d\varepsilon_{xy}(\tau;\ x,0)}{d\tau}\ d\tau \tag{14}$$

where $\varepsilon_{xy}(\tau;\ x,0)$ is shear strain at moment τ in location (x, 0).

To find the strains in equation (14), differentiate with respect to time both sides of equation (2) when $\varepsilon_{ij} = \varepsilon_{xy}$ and $y = 0$:

$$\frac{d\varepsilon_{xy}(\tau;\ x,0)}{d\tau} = \varepsilon^e_{xy}(x,0)\frac{d\Lambda(\tau)}{d\tau} \tag{15}$$

where $\varepsilon^e_{xy}(x,0)$ is elastic shear strain at moment τ in location (x, 0) above crack tip.

Insert equation (15) into equation (14):

$$\sigma_{xy}(t;\ x,0) = \frac{1}{1+\nu}\varepsilon^e_{xy}(x,0)\int_0^t E(t-\tau)\frac{d\Lambda(\tau)}{d\tau}\ d\tau \tag{16}$$

Now examine the time history of loading integral in equation (16). Due to the high frequency ω of traffic loading (in comparison with the relatively slow temperature cycling), the integral in equation (16) can be approximated as follows:

$$\int_0^t E(t-\tau)\frac{d\Lambda(\tau)}{d\tau}\ d\tau\ \approx |E^*|(\omega)\Lambda(t) \tag{17}$$

where $|E^*|(\omega)$ is dynamic modulus of asphalt material determined at frequency ω. Then equation (16) turns into:

$$\sigma_{xy}(t;\ x,0) = \frac{|E^*|}{1+\nu}\varepsilon^e_{xy}(x,0)\Lambda(t) \tag{18}$$

Normalize equation (18) by use of instantaneous modulus $E(0)$ and introduce dimensionless $\bar{E}$:

$$\frac{\sigma_{xy}(t;\ x,0)}{E(0)} = \frac{|E^*|}{E(0)}\frac{1}{1+\nu}\varepsilon^e_{xy}(x,0)\Lambda(t) = \frac{\bar{E}}{1+\nu}\varepsilon^e_{xy}(x,0)\Lambda(t) = \sigma^e_{xy}(x,0)\Lambda(t) \tag{19}$$

At this point, we could insert FEM-computed $\sigma_{xy}(t;\ x,0)$ into equation (14) to get the stress value at each moment in time. To obtain the integral load $P_{VE}(t)$ in equation (13), the whole array of such time-stress curves must be computed at each increment of depth and at each time step. This

process is computationally expensive. Instead, an elastic solution for $\sigma_{xy}^{e}(x, 0)$ was derived and is presented in appendices A and B accompanying this report.

6. CONCLUSIONS

This study derived the modified Paris' law for Mode II fracture in viscoelastic material using the concept of pseudo-energy. The mechanistic response of the structure was derived analytically for the plane strain problem with prescribed vertical boundary displacements due to traffic-induced loading. There are three possible directions for further model development starting from the current stage of modelling.

1. In addition to Mode II fracture, traffic loading induces a Mode I fracture when the center of the wheel load is located directly above the joint, bending both neighboring slabs symmetrically with respect to the joint surface. Such mixed mode loading needs a clear methodology of mode separation for further analysis.

2. The Mode II cracking analysis could be expanded by introducing the third dimension. This would allow consideration of horizontal as well as vertical crack growth (i.e., "channeling" in the transverse direction). Analytically, this is a challenging problem because it is no longer a plane strain problem. Probably, it can be solved only numerically using a finite element method.

3. Mode III (out-of-plane shear cracking) could be added to the consideration of fracture. This would allow analysis of fractures occurring outside of the wheel pathway due to screw dislocation at the joint. In Mode III, the model may be treated analytically in two dimensions as an anti-plane strain problem.

7. REFERENCES

Demidov, A. S. (2001). *Generalized functions in mathematical physics: Main ideas and concepts*. Nova Science Publishers.

Federal Aviation Administration. (n.d.). *Reflective cracking program*. Retrieved May 26, 2021 from https://www.airporttech.tc.faa.gov/Airport-Pavement/National-Airport-Pavement-Test-Facility/Reflective-Cracking-Program.

Gu, F., Luo, X., Zhang, Y., & Lytton, R. L.. (2015). Using overlay test to evaluate fracture properties of field-aged asphalt concrete, *Construction and Building Materials*, *101*(1), 1059–1068. https://doi.org/10.1016/j.conbuildmat.2015.10.159

Hu, S., Hu, X., Zhou, F., & Walubita, L. F. (2008). SA-CrackPro: New finite element analysis tool for pavement crack propagation. *Transportation Research Record: Journal of the Transportation Research Board*, *2068*(1), 10–19. https://doi.org/10.3141%2F2068-02

Tuleubekov K. (2020). *Reflective crack propagation model – part 1: mode 1* (FAA Report DOT/FAA/TC-20/17). https://www.airporttech.tc.faa.gov/Products/Airport-Pavement-Papers-Publications/Airport-Pavement-Detail/ArtMID/3684/ArticleID/2840/Reflective-Crack-Propagation-Model

Walubita, L. F., Faruk, A. N., Koohi, Y., Luo, R., Scullion, T., & Lytton, R. L. (2013).*The overlay tester (OT): Comparison with other crack test methods and recommendations for surrogate crack tests* (Report No. FHWA/TX-13/0-6607-2). Texas Department of Transportation, Research and Technology Implementation Office. http://tti.tamu.edu/documents/0-6607-2.pdf

APPENDIX A—SOLUTION FOR ENTIRE DOMAIN

For mathematical convenience, a small finite distance $\delta > 0$ between slab edges (Figure A-1) is introduced. Besides its obvious physical meaning, this device solves a problem that otherwise would require application of supposed generalized functions (Demidov, 2001), i.e., the discontinuous displacement boundary condition in the vicinity of the joint. To solve this problem, we will use a continuous approximation of the discontinuous boundary (Figure A-2).

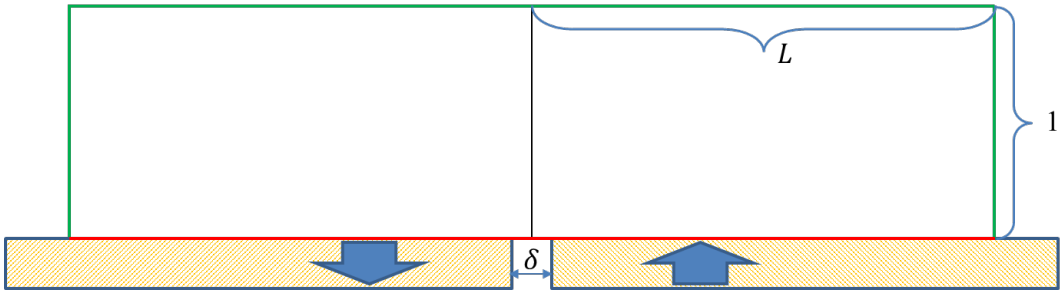

Figure A-1. Undamaged Overlay Under Shear Loading

In dimensionless variables, the boundary conditions are:

$$u_x|_{y=0} = 0 \tag{A.1}$$

$$u_y|_{y=0} = u_0 \begin{cases} x/\delta\,, & |x| \le \delta \\ sign\,(x), & \delta \le |x| \le L \\ 0, & |x| > L \end{cases} \tag{A.2}$$

$$\sigma_{yy}|_{y=1} = 0 \tag{A.3}$$

$$\sigma_{xy}|_{y=1} = 0 \tag{A.4}$$

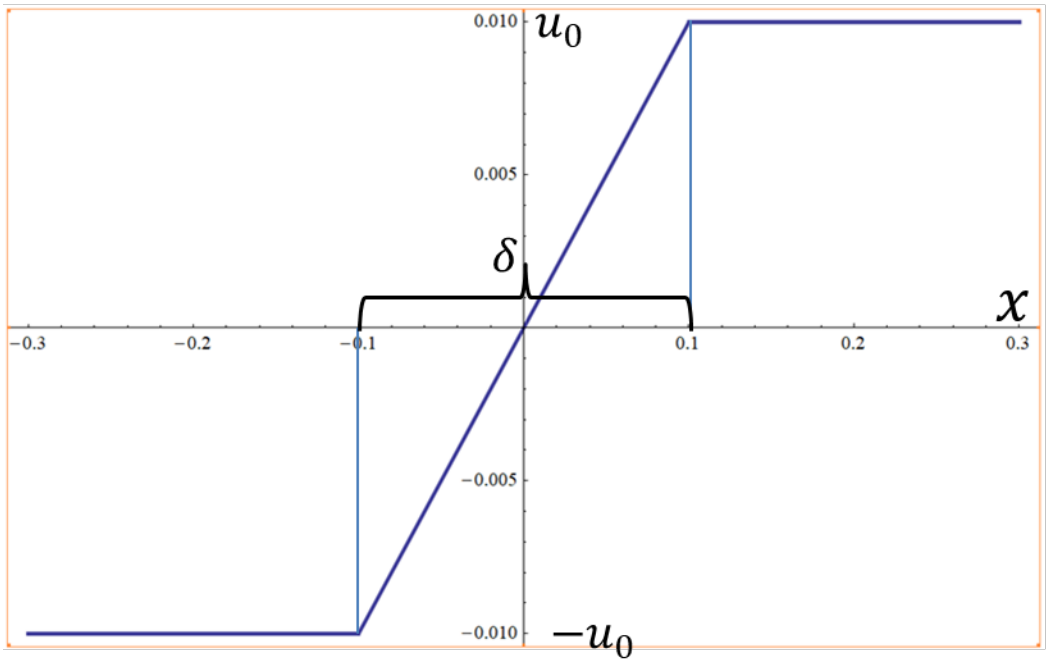

Figure A-2. Continuous Approximation of Boundary Vertical Displacement

Equilibrium equations written in terms of displacements are:

$$\frac{\partial^2 u_x}{\partial x^2}+\frac{\partial^2 u_x}{\partial y^2}+\frac{1}{1-2\nu}\frac{\partial}{\partial x}\left(\frac{\partial u_x}{\partial x}+\frac{\partial u_y}{\partial y}\right)=0 \qquad \text{(A. 5)}$$

$$\frac{\partial^2 u_y}{\partial x^2}+\frac{\partial^2 u_y}{\partial y^2}+\frac{1}{1-2\nu}\frac{\partial}{\partial y}\left(\frac{\partial u_x}{\partial x}+\frac{\partial u_y}{\partial y}\right)=0 \qquad \text{(A. 6)}$$

It can be shown that displacements are taken in the following form:

$$u_x=(1+\nu)\left(-\frac{\partial \Phi_0}{\partial x}-y\frac{\partial \Phi_2}{\partial x}\right) \qquad \text{(A. 7)}$$

$$u_y=(1+\nu)\left(\kappa\Phi_2-\frac{\partial \Phi_0}{\partial y}-y\frac{\partial \Phi_2}{\partial y}\right) \qquad \text{(A. 8)}$$

where $(\kappa=3-4\nu)$ is a solution to the system of equations (A.5) and (A.6), provided that $\Phi_0(x,y),\Phi_2(x,y)$ are harmonic potentials:

$$\frac{\partial^2 \Phi_0}{\partial x^2}+\frac{\partial^2 \Phi_0}{\partial y^2}=0;\qquad \frac{\partial^2 \Phi_2}{\partial x^2}+\frac{\partial^2 \Phi_2}{\partial y^2}=0. \qquad \text{(A. 9)}$$

Stresses in this case are:

$$\sigma_{xx} = -\frac{\partial^2 \Phi_0}{\partial x^2} + 2\nu \frac{\partial \Phi_2}{\partial y} - y\frac{\partial^2 \Phi_2}{\partial x^2} \tag{A.10}$$

$$\sigma_{yy} = \frac{\partial}{\partial y}\left(2(1-\nu)\Phi_2 - \frac{\partial \Phi_0}{\partial y}\right) - y\frac{\partial^2 \Phi_2}{\partial y^2} \tag{A.11}$$

$$\sigma_{xy} = \frac{\partial}{\partial x}\left((1-2\nu)\Phi_2 - \frac{\partial \Phi_0}{\partial y} - y\frac{\partial \Phi_2}{\partial y}\right) \tag{A.12}$$

Thus, to find Φ_0, Φ_2, we seek them in the form of Fourier integrals (Uflyand, 1968):

$$\Phi_0(x,y) = \frac{1}{\sqrt{2\pi}} \int_{-\infty}^{\infty} (A_0(\lambda)\cosh\lambda y + B_0(\lambda)\sinh\lambda y) e^{-i\lambda x}\frac{d\lambda}{\lambda} \tag{A.13}$$

$$\Phi_2(x,y) = \frac{1}{\sqrt{2\pi}} \int_{-\infty}^{\infty} (A_2(\lambda)\cosh\lambda y + B_2(\lambda)\sinh\lambda y) e^{-i\lambda x} d\lambda \tag{A.14}$$

Henceforth, $\hat{f}$ will denote the Fourier transform of f with respect to x:

$$\hat{f}(\lambda) = \frac{1}{\sqrt{2\pi}} \int_{-\infty}^{\infty} f(x) e^{i\lambda x} dx$$

Fourier transforms of each boundary condition are:

$$\widehat{u_x}|_{y=0} = 0 \tag{A.15}$$

$$\widehat{u_y|_{y=0}} = \frac{1}{\sqrt{2\pi}} \int_{-\infty}^{\infty} u_y(x) e^{i\lambda x} dx = \sqrt{\frac{2}{\pi}}\frac{iu_0}{\delta\lambda^2}\ (\sin\delta\lambda - \delta\lambda\cos L\lambda) \tag{A.16}$$

$$\widehat{\sigma_{yy}}\big|_{y=1} = 0 \tag{A.17}$$

$$\widehat{\sigma_{xy}}\big|_{y=1} = 0 \tag{A.18}$$

Fourier transforms of potentials (A.13) and (A.14) are:

$$\widehat{\Phi_0}(\lambda,y) = \frac{1}{\lambda}(A_0(\lambda)\cosh\lambda y + B_0(\lambda)\sinh\lambda y) \tag{A.19}$$

$$\widehat{\Phi_2}(\lambda,y) = A_2(\lambda)\cosh\lambda y + B_2(\lambda)\sinh\lambda y \tag{A.20}$$

Transform (A.7-A.8) and (A.11-A.13), then use the transformed boundary conditions (A.16-A.18):

$$\widehat{\Phi_0}\big|_{y=0} = 0 \tag{A.21}$$

$$(1+\nu)\left(\kappa\widehat{\Phi_2} - \frac{\partial\widehat{\Phi_0}}{\partial y}\right)\Big|_{y=0} = \sqrt{\frac{2}{\pi}}\,\frac{iu_0}{\delta\lambda^2}\;(\sin\delta\lambda - \delta\lambda\cos L\lambda) \tag{A.22}$$

$$\left(\frac{\partial}{\partial y}\left(2(1-\nu)\widehat{\Phi_2} - \frac{\partial\widehat{\Phi_0}}{\partial y}\right) - y\frac{\partial^2\widehat{\Phi_2}}{\partial y^2}\right)\Big|_{y=1} = 0 \tag{A.23}$$

$$\left((1-2\nu)\widehat{\Phi_2} - \frac{\partial\widehat{\Phi_0}}{\partial y} - y\frac{\partial\widehat{\Phi_2}}{\partial y}\right)\Big|_{y=1} = 0 \tag{A.24}$$

Solving (A.21-A.24) with respect to A_0, A_2, B_0, B_2:

$$A_0(\lambda) = 0 \tag{A.25}$$

$$A_2(\lambda) = \sqrt{\frac{2}{\pi}}\frac{iu_0(\cosh(2\lambda)+3-4\nu)(\sin(\delta\lambda)-\delta\lambda\cos(L\lambda))}{\delta\lambda^2(\nu+1)(2\lambda^2+(3-4\nu)\cosh(2\lambda)+8\nu^2-12\nu+5)} \tag{A.26}$$

$$B_0(\lambda) = \sqrt{\frac{2}{\pi}}\frac{2iu_0(\lambda^2-4\nu^2+6\nu-2)(\delta\lambda\cos(L\lambda)-\sin(\delta\lambda))}{\delta\lambda^2(\nu+1)(2\lambda^2+(3-4\nu)\cosh(2\lambda)+8\nu^2-12\nu+5)} \tag{A.27}$$

$$B_2(\lambda) = \sqrt{\frac{2}{\pi}}\frac{iu_0(\sinh(2\lambda)-2\lambda)(\delta\lambda\cos(L\lambda)-\sin(\delta\lambda))}{\delta\lambda^2(\nu+1)(2\lambda^2+(3-4\nu)\cosh(2\lambda)+8\nu^2-12\nu+5)} \tag{A.28}$$

For short notation, extract the common factor in (A.26-A.28):

$$\Psi(\lambda) = \frac{\delta\lambda\cos(L\lambda)-\sin(\delta\lambda)}{\delta\lambda^2(\nu+1)(2\lambda^2+(3-4\nu)\cosh(2\lambda)+8\nu^2-12\nu+5)} \tag{A.29}$$

Note that (A.29) is an odd function with respect to λ:

$$\Psi(-\lambda) = -\Psi(\lambda) \tag{A.30}$$

Rewrite (A.26-A.28) in terms of $\Psi(\lambda)$:

$$A_0(\lambda) = 0$$

$$A_2(\lambda) = -iu_0\sqrt{\frac{2}{\pi}}(\cosh(2\lambda) + 3 - 4\nu)\Psi(\lambda) \tag{A.31}$$

$$B_0(\lambda) = 2iu_0\sqrt{\frac{2}{\pi}}(\lambda^2 - 4\nu^2 + 6\nu - 2)\Psi(\lambda) \tag{A.32}$$

$$B_2(\lambda) = iu_0\sqrt{\frac{2}{\pi}}(\sinh(2\lambda) - 2\lambda)\Psi(\lambda) \tag{A.33}$$

The first potential is:

$$\Phi_0 = \frac{1}{\sqrt{2\pi}}\int_{-\infty}^{\infty} B_0(\lambda)\frac{\sinh\lambda y}{\lambda}e^{-i\lambda x}d\lambda \tag{A.34}$$

Due to (A.30), the integrand in (A.34) is odd with respect to integration variable λ:

$$B_0(-\lambda)\frac{\sinh(-\lambda y)}{-\lambda} = -B_0(\lambda)\frac{\sinh\lambda y}{\lambda} \tag{A.35}$$

Therefore, the cosine part of the transform vanishes:

$$\begin{aligned}\int_{-\infty}^{\infty} B_0(\lambda)\frac{\sinh\lambda y}{\lambda}(\cos\lambda x - i\sin\lambda x)d\lambda &= -i\int_{-\infty}^{\infty} B_0(\lambda)\frac{\sinh\lambda y}{\lambda}\sin\lambda x\, d\lambda \\ &= -2i\int_0^{\infty} B_0(\lambda)\frac{\sinh\lambda y}{\lambda}\sin\lambda x\, d\lambda \\ &= 4u_0\sqrt{\frac{2}{\pi}}\int_0^{\infty}\frac{\sinh\lambda y}{\lambda}(\lambda^2 - 4\nu^2 + 6\nu - 2)\Psi(\lambda)\sin\lambda x\, d\lambda\end{aligned}$$

Thus:

$$\Phi_0 = \frac{4u_0}{\pi}\int_0^{\infty}\sin\lambda x\frac{\sinh\lambda y}{\lambda}(\lambda^2 - 4\nu^2 + 6\nu - 2)\Psi(\lambda)d\lambda \tag{A.36}$$

Differentiate (A.36) with respect to *x*:

$$\frac{\partial \Phi_0}{\partial \mathrm{x}} = \frac{4u_0}{\pi} \int_0^\infty \cos \lambda x \sinh \lambda y \, (\lambda^2 - 4\nu^2 + 6\nu - 2)\Psi(\lambda) d\lambda \qquad \text{(A. 37)}$$

$$\frac{\partial^2 \Phi_0}{\partial x^2} = -\frac{4u_0}{\pi} \int_0^\infty \lambda \sin \lambda x \sinh \lambda y \, (\lambda^2 - 4\nu^2 + 6\nu - 2)\Psi(\lambda) d\lambda \qquad \text{(A. 38)}$$

Now differentiate with respect to *y*:

$$\frac{\partial \Phi_0}{\partial \mathrm{y}} = \frac{4u_0}{\pi} \int_0^\infty \sin \lambda x \cosh \lambda y \, (\lambda^2 - 4\nu^2 + 6\nu - 2)\Psi(\lambda) d\lambda \qquad \text{(A. 39)}$$

$$\frac{\partial^2 \Phi_0}{\partial y^2} = \frac{4u_0}{\pi} \int_0^\infty \lambda \sin \lambda x \sinh \lambda y \, (\lambda^2 - 4\nu^2 + 6\nu - 2)\Psi(\lambda) d\lambda \qquad \text{(A. 40)}$$

Verify that Φ_0 is harmonic, i.e., its Laplacian must be zero:

$$\frac{\partial^2 \Phi_0}{\partial x^2} + \frac{\partial^2 \Phi_0}{\partial y^2} = -\frac{4u_0}{\pi} \int_0^\infty \lambda \sin \lambda x \sinh \lambda y \, (\lambda^2 - 4\nu^2 + 6\nu - 2)\Psi(\lambda) d\lambda + \frac{4u_0}{\pi} \int_0^\infty \lambda \sin \lambda x \sinh \lambda y \, (\lambda^2 - 4\nu^2 + 6\nu - 2)\Psi(\lambda) d\lambda = 0$$

Now, consider the second potential (A.14). As observed from (A.31) and (A.33) using (A.30):

$$A_2(-\lambda) = -A_2(\lambda), \qquad B_2(-\lambda) = B_2(\lambda)$$

Therefore, the integrand in $\Phi_2(x, y)$ is an odd function with respect to λ, as shown below:

$$A_2(-\lambda)\cosh(-\lambda y) + B_2\,(-\lambda)\sinh(-\lambda y) = -A_2(\lambda)\cosh(\lambda y) - B_2\,(\lambda)\sinh(\lambda y) \qquad \text{(A. 41)}$$

This implies that the cosine part of integral (A.14) vanishes:

$$\int_{-\infty}^{\infty} (A_2(\lambda)\cosh\lambda y + B_2(\lambda)\sinh\lambda y)(\cos\lambda x - i\sin\lambda x)d\lambda =$$

$$= -2i\int_{0}^{\infty} (A_2(\lambda)\cosh\lambda y + B_2(\lambda)\sinh\lambda y)\sin\lambda x\, d\lambda$$

$$= 2u_0\sqrt{\frac{2}{\pi}}\int_{0}^{\infty} \Psi(\lambda)\ (-(\cosh(2\lambda) + 3 - 4\nu)\cosh\lambda y + (\sinh(2\lambda) - 2\lambda)\sinh\lambda y)\sin\lambda x\, d\lambda$$

Thus:

$$\Phi_2(x,y) = \frac{2u_0}{\pi}\int_{0}^{\infty} \Psi(\lambda)\ (-\kappa\cosh y\lambda - 2\lambda\sinh y\lambda - \cosh\ \lambda(y-2))\sin\lambda x\, d\lambda\ . \text{(B. 42)}$$

Differentiate (A.42) along the *x* variable:

$$\frac{\partial\Phi_2}{\partial \mathrm{x}} = \frac{2u_0}{\pi}\int_{0}^{\infty} \Psi(\lambda)\ (-\kappa\cosh y\lambda - 2\lambda\sinh y\lambda - \cosh\ \lambda(y-2))\lambda\cos\lambda x\, d\lambda \qquad \text{(A. 43)}$$

$$\frac{\partial^2\Phi_2}{\partial x^2} = \frac{2u_0}{\pi}\int_{0}^{\infty} \Psi(\lambda)\ (\kappa\cosh y\lambda + 2\lambda\sinh y\lambda + \cosh\ \lambda(y-2))\lambda^2\sin\lambda x\, d\lambda \qquad \text{(A. 44)}$$

Differentiate along *y*:

$$\frac{\partial\Phi_2}{\partial \mathrm{y}} = \frac{2u_0}{\pi}\int_{0}^{\infty} \Psi(\lambda)\ \lambda(-\kappa\sinh y\lambda - 2\lambda\cosh y\lambda - \sinh\ \lambda(y-2))\sin\lambda x\, d\lambda \qquad \text{(A. 45)}$$

$$\frac{\partial^2\Phi_2}{\partial y^2} = \frac{2u_0}{\pi}\int_{0}^{\infty} \Psi(\lambda)\ \lambda^2(-\kappa\cosh y\lambda - 2\lambda\sinh y\lambda - \cosh\ \lambda(y-2))\sin\lambda x\, d\lambda \qquad \text{(A. 46)}$$

Verify that Φ_2 is harmonic, i.e., its Laplacian must be zero:

$$\frac{\partial^2\Phi_2}{\partial x^2} + \frac{\partial^2\Phi_2}{\partial y^2} = \frac{2u_0}{\pi}\int_{0}^{\infty} \Psi(\lambda)\ (\kappa\cosh y\lambda + 2\lambda\sinh y\lambda + \cosh\ \lambda(y-2))\lambda^2\sin\lambda x\, d\lambda$$

$$+ \frac{2u_0}{\pi}\int_{0}^{\infty} \Psi(\lambda)\ \lambda^2(-\kappa\cosh y\lambda - 2\lambda\sinh y\lambda - \cosh\ \lambda(y-2))\sin\lambda x\, d\lambda = 0$$

Compute u_x from (A.7) using derivatives (A.37) and (A.43). First:

$$-\frac{\partial \Phi_0}{\partial x} - y\frac{\partial \Phi_2}{\partial x} =$$
$$= -\frac{4u_0}{\pi}\int_0^\infty \cos\lambda x \sinh\lambda y\,(\lambda^2 - 4\nu^2 + 6\nu - 2)\Psi(\lambda)d\lambda$$
$$+\frac{2u_0}{\pi}\int_0^\infty \Psi(\lambda)\ y(\kappa\cosh y\lambda + 2\lambda\sinh y\lambda + \cosh\lambda(y-2))\lambda\cos\lambda x\,d\lambda$$
$$= \frac{2u_0}{\pi}\int_0^\infty \Psi(\lambda)\ \{-2\sinh\lambda y\,(\lambda^2 - 4\nu^2 + 6\nu - 2)$$
$$+\lambda y(\kappa\cosh y\lambda + 2\lambda\sinh y\lambda + \cosh\lambda(y-2))\}\cos\lambda x\,d\lambda$$

Thus, horizontal displacement:

$$u_x(x,y) = \frac{2u_0}{\pi}\int_0^\infty \frac{(\delta\lambda\cos(L\lambda) - \sin\delta\lambda)\cos\lambda x}{\delta\lambda^2(2\lambda^2 + \kappa\cosh(2\lambda) + 8\nu^2 - 12\nu + 5)}\{-2\sinh\lambda y\,(\lambda^2 - 4\nu^2 + 6\nu - 2)$$
$$+\lambda y(\kappa\cosh y\lambda + 2\lambda\sinh y\lambda + \cosh\lambda(y-2))\}\,d\lambda \qquad \text{(A. 47)}$$

Then in a similar way, compute vertical displacement u_y from equation (A.8) using equations (A.39), (A.42), and (A.45):

$$u_y(x,y) = \frac{2u_0}{\pi}\int_0^\infty \frac{(\delta\lambda\cos(L\lambda) - \sin\delta\lambda)\sin\lambda x}{\delta\lambda^2(2\lambda^2 + \kappa\cosh(2\lambda) + 8\nu^2 - 12\nu + 5)}\{(2(y-1)\lambda^2 - 8\nu^2 + 12\nu$$
$$-5)\cosh y\lambda + \lambda(y\sinh(y-2)\lambda + (y-2)\kappa\sinh y\lambda) - \kappa\cosh(y-2)\lambda)\}\,d\lambda \qquad \text{(A. 48)}$$

Now derive the stresses in (A.11) and (A.12). First, (A.11):

$$\sigma_{yy} = \frac{2u_0}{\pi}\int_0^\infty \frac{(\delta\lambda\cos(L\lambda) - \sin\delta\lambda)\sin\lambda x}{\delta\lambda(\nu+1)(2\lambda^2 + \kappa\cosh(2\lambda) + 8\nu^2 - 12\nu + 5)}\Big[2\Big(\big((y-1)\lambda^2 + \nu$$
$$-1\big)\sinh(y\lambda) + (\nu-1)\sinh\big((y-2)\lambda\big)\Big) + \lambda(\kappa y + 4\nu - 4)\cosh(y\lambda)$$
$$+ y\lambda\cosh\big((y-2)\lambda\big)\Big]\,d\lambda \qquad \text{(A. 49)}$$

Next, derive the stress in (A.12):

$$\sigma_{xy}(x,y) = \frac{2u_0}{\pi}\int_0^\infty \frac{(\delta\lambda\ \cos(L\lambda) - \sin\delta\lambda)\cos\lambda x}{\delta\lambda(\nu+1)(2\lambda^2+\kappa\cosh(2\lambda)+8\nu^2-12\nu+5)}\{(2(y-1)\lambda^2-2\nu + 1)\cosh y\lambda + \lambda\left((\kappa y+4\nu-2)\sinh y\lambda + y\sinh(y-2)\lambda\right) + (2\nu-1)\cosh(y-2)\lambda\}d\lambda \quad (A.50)$$

Now, inserting Φ_0, Φ_2 into (A.10):

$$\sigma_{xx}(x,y) = -\frac{2u_0}{\pi}\int_0^\infty \frac{(\delta\lambda\cos(L\lambda) - \sin\delta\lambda)\sin\lambda x}{\delta\lambda(\nu+1)(2\lambda^2+\kappa\cosh(2\lambda)+8\nu^2-12\nu+5)}\left\{2\left(\left((y-1)\lambda^2-3\nu + 2\right)\sinh y\lambda + \nu\sinh(y-2)\lambda\right) + \lambda(\kappa y+4\nu)\cosh y\lambda + y\lambda\ \cosh(y-2)\lambda\right\}d\lambda \quad (A.52)$$

Verify that the derived displacements in (A.47) and (A.48) satisfy boundary conditions at $y = 0$:

$$u_x(x,0) = \frac{2u_0}{\pi}\int_0^\infty \frac{(\delta\lambda\cos(L\lambda) - \sin\delta\lambda)\cos\lambda x}{\delta\lambda^2(2\lambda^2+\kappa\cosh(2\lambda)+8\nu^2-12\nu+5)}\ 0\ d\lambda = 0 \quad (A.53)$$

$$u_y(x,0) = \frac{2u_0}{\pi}\int_0^\infty \frac{(\delta\lambda\cos(L\lambda) - \sin\delta\lambda)\sin\lambda x}{\delta\lambda^2(2\lambda^2+\kappa\cosh(2\lambda)+8\nu^2-12\nu+5)}\{(-2\lambda^2-8\nu^2+12\nu-5) - \kappa\cosh 2\lambda)\}\ d\lambda = \frac{2u_0}{\pi}\int_0^\infty \frac{-(\delta\lambda\cos(L\lambda) - \sin\delta\lambda)\sin\lambda x}{\delta\lambda^2}\ d\lambda =$$

$$= \frac{u_0}{\pi} i \int_{-\infty}^{\infty} \frac{(\delta\lambda\cos(L\lambda) - \sin\delta\lambda) i\sin\lambda x}{\delta\lambda^2}\ d\lambda =$$

$$= \frac{u_0}{\pi} i \int_{-\infty}^{\infty} \frac{(\sin\delta\lambda - \delta\lambda\cos(L\lambda))}{\delta\lambda^2}\ e^{-i\lambda x} d\lambda =$$

$$= \frac{1}{\sqrt{2\pi}}\int_{-\infty}^{\infty}\sqrt{\frac{2}{\pi}}\ \frac{iu_0}{\delta\lambda^2}\ (\sin\delta\lambda - \delta\lambda\cos L\lambda)\ \ e^{-i\lambda x} d\lambda =$$

$$= u_0\begin{cases} x/\delta\,, & |x| \le \delta \\ sign\,(x), & \delta \le |x| \le L \\ 0, & |x| > L \end{cases} \quad (A.54)$$

In this step, we verified that the displacements (A.47) and (A.48) satisfy both boundary conditions (A.1) and (A.2), as well as the governing equations.

Verify that derived stresses satisfy zero traction boundary conditions at $y = 1$:

$$\sigma_{yy}(x,1) = \frac{2u_0}{\pi}\int_0^\infty \frac{(\delta\lambda\cos(L\lambda) - \sin(\delta\lambda))\sin\lambda x\, 0d\lambda}{\delta\lambda(\nu+1)(2\lambda^2 + \kappa\cosh(2\lambda) + 8\nu^2 - 12\nu + 5)} = 0 \qquad (A.55)$$

$$\sigma_{xy}(x,1) = \frac{2u_0}{\pi}\int_0^\infty \frac{(\delta\lambda\cos(L\lambda) - \sin(\delta\lambda))\cos\lambda x}{\delta\lambda(\nu+1)(2\lambda^2 + \kappa\cosh(2\lambda) + 8\nu^2 - 12\nu + 5)} \{(-2\nu+1)\cosh\lambda + \lambda((\kappa + 4\nu - 2)\sinh\lambda - \sinh\lambda) + (2\nu - 1)\cosh\lambda\}d\lambda = 0 \qquad (B.56)$$

For certain applications it is useful to derive the shear stress $t_c(y) = \sigma_{xy}(0,y)$ along the vertical crack axis at $x = 0$. From equation (A.50), it follows that:

$$\sigma_{xy}(0,y) = \frac{2u_0}{\pi}\int_0^\infty \frac{(\delta\lambda\ \cos(L\lambda) - \sin\delta\lambda)}{\delta\lambda(\nu+1)(2\lambda^2 + \kappa\cosh(2\lambda) + 8\nu^2 - 12\nu + 5)} \{(2(y-1)\lambda^2 - 2\nu + 1)\cosh y\lambda + \lambda\,((\kappa y + 4\nu - 2)\sinh y\lambda + y\sinh(y-2)\lambda) + (2\nu - 1)\cosh(y-2)\lambda\}d\lambda \qquad (A.57)$$

If the joint spacing $\delta \to 0$ between concrete slabs is negligibly small, the stress (A.57) yields:

$$t_c(y) = \lim_{\delta\to 0}\sigma_{xy}(0,y) = \frac{2u_0}{\pi(\nu+1)}\int_0^\infty (\cos(L\lambda) - 1)\ T(y,\nu;\ \lambda)d\lambda \qquad (A.58)$$

where:

$$T(y,\nu;\ \lambda) = \frac{(2(y-1)\lambda^2 - 2\nu + 1)\cosh y\lambda}{2\lambda^2 + \kappa\cosh(2\lambda) + 8\nu^2 - 12\nu + 5} + \frac{\lambda\left((\kappa y + 4\nu - 2)\sinh y\lambda + y\sinh(y-2)\lambda\right)}{2\lambda^2 + \kappa\cosh(2\lambda) + 8\nu^2 - 12\nu + 5} + \frac{(2\nu - 1)\cosh(y-2)\lambda}{2\lambda^2 + \kappa\cosh(2\lambda) + 8\nu^2 - 12\nu + 5} \qquad (A.59)$$

Separate (A.58) into two integrals:

$$t_c(y) = \frac{2u_0}{\pi(\nu+1)}(I_1 + I_2) \qquad (A.60)$$

where:

$$I_1 = -\int_0^\infty T(y,\nu;\ \lambda)\ d\lambda\,; \qquad I_2 = \int_0^\infty \cos(L\lambda)\ T(y,\nu;\ \lambda)\,d\lambda \qquad (A.61)$$

Since $\cos(L\lambda)$ is highly oscillatory on $[0,\infty)$ for sufficiently large slab lengths $L > 10$ (figure A-3), it follows that I_2 is close to zero and much smaller than I_1.

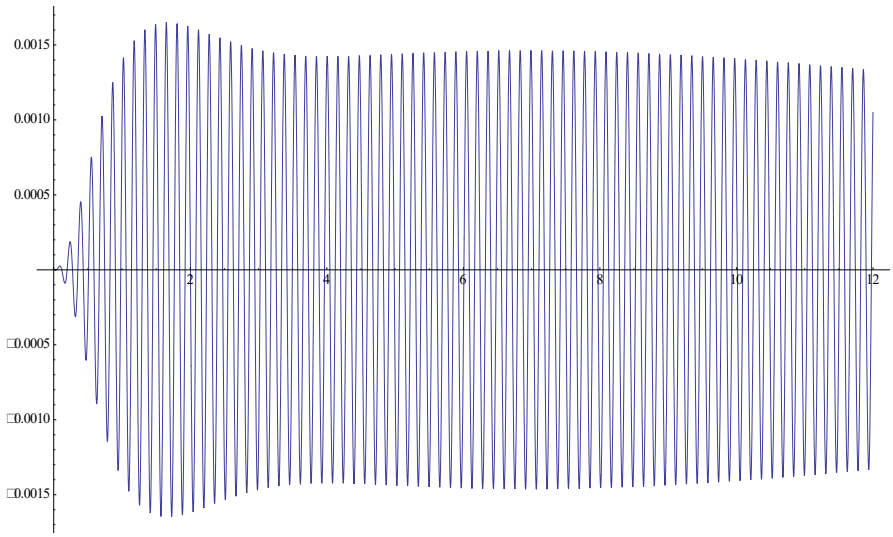

Figure A-3. Integrand of I_2 when $L = 40$

Therefore, for thin slabs we can approximate (A.60) as follows:

$$t_c(y) \approx \frac{2u_0}{\pi(\nu+1)} I_1(y,\nu) \tag{A.62}$$

The function $T(y,\nu;\ \lambda)$ in (A.59) has an asymptote $T_{as}(y,\nu;\ \lambda)$ as $\lambda \to \infty$ as follows:

$$\begin{aligned} T(y,\nu;\ \lambda) \sim & T_{as}(y,\nu;\ \lambda) \\ &= \frac{e^{(y-2)\lambda}(2(y-1)\lambda^2 - 2\nu + 1)}{3-4\nu} + \frac{(2\nu-1)e^{-y\lambda}}{3-4\nu} \\ &+ \frac{2e^{-2\lambda}\lambda(\frac{1}{2}(e^{y\lambda} - e^{-y\lambda})(-4y\nu + 3y + 4\nu - 2) + \frac{1}{2}y(e^{(y-2)\lambda} - e^{(2-y)\lambda}))}{3-4\nu} \end{aligned} \tag{A.63}$$

The asymptote (A.63) provides an asymptote $I_{1,as}$ for the integral I_1 in (A.61) after performing the following integration:

$$\begin{aligned} I_{1,as}(y,\nu) = -\int_0^\infty T_{as}(y,\nu;\ \lambda)\ d\lambda = \\ = \frac{2(y-1)}{(y-4)^2(y-2)^3 y(y+2)^2(3-4\nu)} \Big(2\Big(\big((y-8)y+8\big)y^2+16\Big)(y-4)^2\nu \\ - y^2\big(y\big(y\big((y-22)y+128\big)-280\big)+144\big)-512\Big) \end{aligned} \tag{A.64}$$

Despite the simplicity of formula (A.64) for $I_{1,as}$, it approximates I_1 quite accurately (figure A-4).

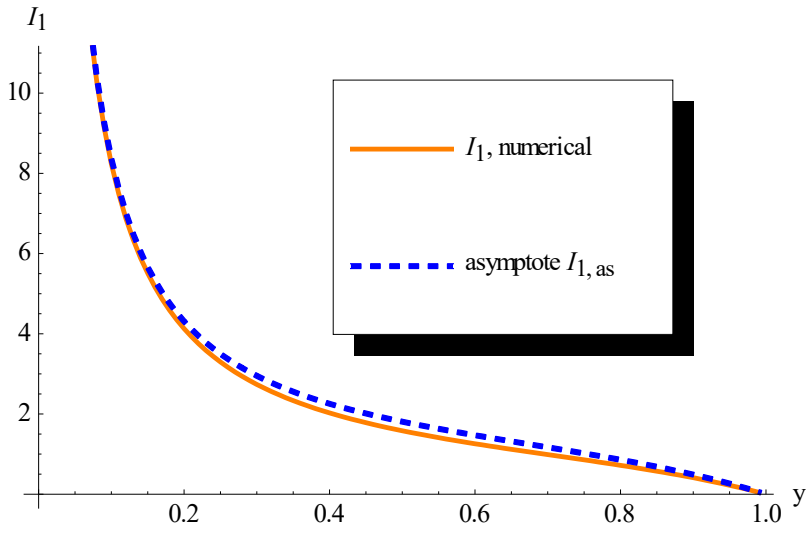

Figure A-4. Comparison of I_1 (solid) vs $I_{1,as}$ (dashed) When $\nu = 0.35$

Inserting (A.64) into (A.62), the shear stress from (A.60) can be computed approximately as follows:

$$t_c(y) = \frac{2u_0}{\pi(\nu+1)} \frac{2(y-1)}{(y-4)^2(y-2)^3 y(y+2)^2(3-4\nu)} \Big(2\Big(\big((y-8)y+8\big)y^2+16\Big)(y-4)^2\nu - y^2\big(y\big(y\big((y-22)y+128\big)-280\big)+144\big)-512\Big) \tag{A.65}$$

Formula (A.65) provides the solution to the problem in the uncracked domain when boundary vertical displacements are prescribed.

REFERENCE

Uflyand, Ja. S. (1968). *Integral transforms in problems of elasticity theory* [in Russian], 2nd edition. Nauka, Leningrad.

APPENDIX B—STRESS INTENSITY FACTOR FOR EDGE CRACK

Following the solution for the full domain (Appendix A), the next step is to solve problem A (figure B-1) where: (1) the displacement on the bottom surface ($y = 0$) is zero, and (2) the crack faces are loaded by shear stresses $-t_c(y)$ in the opposite direction to the shear stress at the crack location in the uncracked material.

Note that t_c does not depend on crack length.

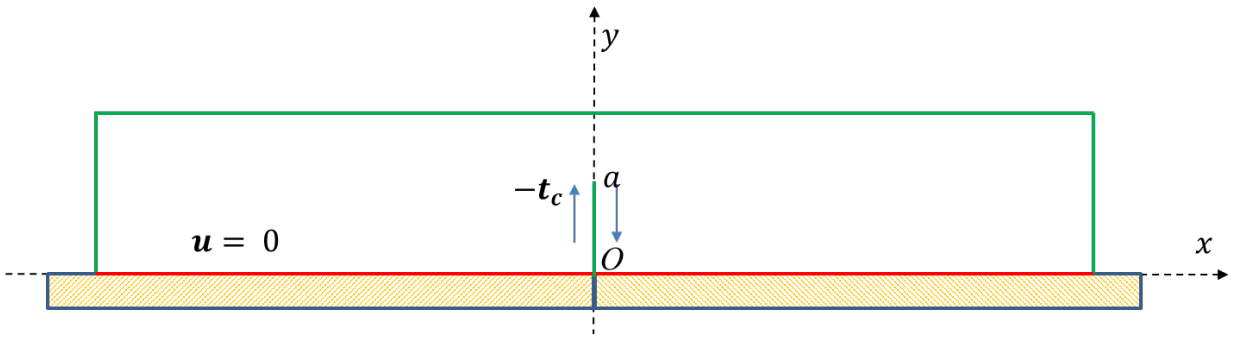

Figure B-1. Problem A with Edge Crack

To solve problem A for an edge crack of length a, we extend the domain of the original problem by reflecting it on $y = 0$. To maintain zero displacement at $y = 0$, we reflect the tractions onto the reflected crack as follows:

$$t_c(-y) = -t_c(y) \tag{B.1}$$

As a result, problem B has an internal crack of length $2a$. The stress intensity factor (SIF) at the upper tip of this internal crack will be the same as in problem A.

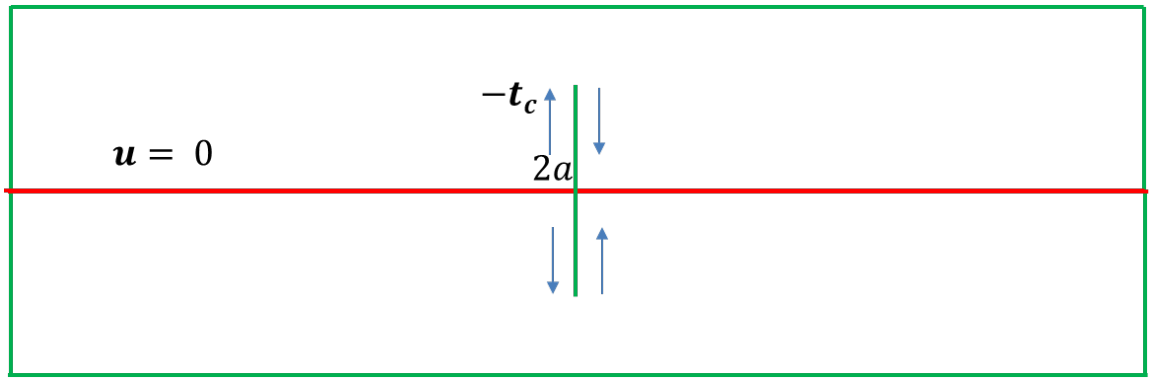

Figure B-2. Problem B with Internal Crack

For an internal crack, the SIFs are well-known from the literature (Sun & Jin, 2012):

$$K_{II} = \frac{1}{\sqrt{\pi a}} \int_{-a}^{a} t_c(y) \sqrt{\frac{a+y}{a-y}}\, dy \tag{B.2}$$

Substituting the property (B.1) into (B.2) yields:

$$\begin{aligned} K_{II} &= \frac{1}{\sqrt{\pi a}} \left(\int_{-a}^{0} t_c(y) \sqrt{\frac{a+y}{a-y}}\, dy + \int_{0}^{a} t_c(y) \sqrt{\frac{a+y}{a-y}}\, dy \right) = \\ &= \frac{1}{\sqrt{\pi a}} \left(-\int_{a}^{0} t_c(-y) \sqrt{\frac{a-y}{a+y}}\, dy + \int_{0}^{a} t_c(y) \sqrt{\frac{a+y}{a-y}}\, dy \right) = \\ &= \frac{1}{\sqrt{\pi a}} \int_{0}^{a} dy \left(-t_c(y) \sqrt{\frac{a-y}{a+y}} + t_c(y) \sqrt{\frac{a+y}{a-y}} \right) = \\ &= \frac{1}{\sqrt{\pi a}} \int_{0}^{a} t_c(y) \left(\sqrt{\frac{a+y}{a-y}} - \sqrt{\frac{a-y}{a+y}} \right) dy \end{aligned} \tag{B.3}$$

Finally, inserting the stress (B.1) into the expression in (B.3) gives the SIF for Mode II. Table B-1 compares the results of (B.3) to the finite element model (FEM) analysis in ABAQUS software of the same problem. when elastic modulus is equal to one and Poisson's ratio $\nu = 0.35$

Table B-1. Comparison of Mode II SIFs from FEM and Equation (B.3)

Crack Length, a/h	K_{II}, FEM [Pa √m]	K_{II}, (C.2) Numerical [Pa √m]
0.1	-0.019	-0.021
0.2	-0.0135	-0.0156
0.3	-0.0109	-0.0118
0.4	-0.0095	-0.0111
0.5	-0.0085	-0.0092
0.6	-0.00792	-0.0090
0.7	-0.00750	-0.0075
0.8	-0.00736	-0.00731

Additionally:

$$K_{II} = \frac{2u_0}{\pi\sqrt{\pi a}(\nu+1)} \int_{0}^{a} I_1(y,\nu) \left(\sqrt{\frac{a+y}{a-y}} - \sqrt{\frac{a-y}{a+y}} \right) dy \tag{B.4}$$

Inserting $I_{1,as}$ from (A.64) into (B.4) yields:

$$K_{II} = \frac{2u_0}{\pi\sqrt{\pi a}(\nu+1)}\int_0^a \frac{2(y-1)}{(y-4)^2(y-2)^3y(y+2)^2(3-4\nu)}\Big(2\Big(\big((y-8)y+8\big)y^2+16\Big)(y-4)^2\nu - y^2\big(y\big(y\big((y-22)y+128\big)-280\big)+144\big)-512\Big)\left(\sqrt{\frac{a+y}{a-y}}-\sqrt{\frac{a-y}{a+y}}\right)dy =$$

$$-\frac{1}{(a-4)(a+4)(4\nu-3)d_1^2\sqrt{ad_3}}2\Big(16\big(64\sqrt{a^3d_3}-20\sqrt{a^7d_3}+\sqrt{a^{11}d_3}\big)\nu+3072i\log(2)\sqrt{ad_2}\nu - 1024\pi\sqrt{ad_2}\nu-2752i\log(2)\sqrt{a^5d_2}\nu+832\pi\sqrt{a^5d_2}\nu+608i\log(2)\sqrt{a^9d_2}\nu - 176\pi\sqrt{a^9d_2}\nu-28i\log(2)\sqrt{a^{13}d_2}\nu+8\pi\sqrt{a^{13}d_2}\nu-512\pi\sqrt{ad_3}\nu+288\pi\sqrt{a^5d_3}\nu - 48\pi\sqrt{a^9d_3}\nu+2\pi\sqrt{a^{13}d_3}\nu+8i\log\big(a+i\sqrt{d_2}\big)\Big(128\sqrt{ad_1}-80\sqrt{a^5d_1}+16\sqrt{a^9d_1} - \sqrt{a^{13}d_1}\Big)+10i\log(2-a)\Big(2\nu\Big(-128\sqrt{ad_2}+104\sqrt{a^5d_2}-22\sqrt{a^9d_2}+\sqrt{a^{13}d_2}\Big) - 192\sqrt{a^5d_2}+27\sqrt{a^9d_2}-\sqrt{a^{13}d_2}\Big)+2i\log(-(a-2)^5)\Big(\nu\Big(256\sqrt{ad_2}-208\sqrt{a^5d_2}+ 44\sqrt{a^9d_2}-2\sqrt{a^{13}d_2}\Big)-256\sqrt{ad_2}+192\sqrt{a^5d_2}-27\sqrt{a^9d_2}+\sqrt{a^{13}d_2}\Big)+ 2i\Big(1280\sqrt{ad_2}\log\Big(-(a-2)\big(a+i\sqrt{d_1}\big)\Big)+\log\big(a+i\sqrt{d_1}\big)\Big(-2\nu\Big(768\sqrt{ad_2}-688\sqrt{a^5d_2}+ 152\sqrt{a^9d_2}-7\sqrt{a^{13}d_2}\Big)-1072\sqrt{a^5d_2}+206\sqrt{a^9d_2}-9\sqrt{a^{13}d_2}\Big)\Big)-1024i\log(4)\sqrt{ad_1}+ 1024\pi\sqrt{ad_1}+640i\log(4)\sqrt{a^5d_1}-640\pi\sqrt{a^5d_1}-128i\log(4)\sqrt{a^9d_1}+128\pi\sqrt{a^9d_1}+ 8i\log(4)\sqrt{a^{13}d_1}-8\pi\sqrt{a^{13}d_1}-2560i\log(2)\sqrt{ad_2}+1024\pi\sqrt{ad_2}+2144i\log(2)\sqrt{a^5d_2}- 768\pi\sqrt{a^5d_2}-412i\log(2)\sqrt{a^9d_2}+108\pi\sqrt{a^9d_2}+18i\log(2)\sqrt{a^{13}d_2}-4\pi\sqrt{a^{13}d_2}+ 256\pi\sqrt{ad_3}-704\sqrt{a^3d_3}-144\pi\sqrt{a^5d_3}+184\sqrt{a^7d_3}+24\pi\sqrt{a^9d_3}-11\sqrt{a^{11}d_3}- \pi\sqrt{a^{13}d_3}\Big) \tag{B.5}$$

where $i=\sqrt{-1}$ and

$$d_1 = 4-a^2, \qquad d_2 = 16-a^2, \qquad d_3 = a^4-20a^2+64 \tag{B.6}$$

REFERENCE

Sun, C.T., & Jin, Z. -H.,(2012). *Fracture mechanics*. Elsevier. https://doi.org/10.1016/C2009-0-63512-1